chemistry

MDPI

Article

A Stable π-Expanded *o*-Quinodimethane via the Photochemical Dearomative Cycloaddition of Corannulene with an Isolable Dialkylsilylene

Shintaro Ishida *, Maiko Mori, Shunya Honda and Takeaki Iwamoto *

Department of Chemistry, Graduate School of Science, Tohoku University, Aoba-ku, Sendai 980-8578, Japan
* Correspondence: ishida@tohoku.ac.jp (S.I.); takeaki.iwamoto@tohoku.ac.jp (T.I.)

Abstract: A stable π-expanded *o*-quinodimethane derivative (**2**) was synthesized by photochemical dearomative cycloaddition of corannulene with an isolable dialkylsilylene (**1**) and isolated as a dark blue solid. Compound **2** adopts a very flat bowl shape in contrast to parent corannulene. Structural and spectroscopic characteristics, redox properties, and computational study suggest that **2** has a small but significant diradical character ($y_0 = 0.11$). One-electron reduction of **2** provides the corresponding radical anion as an isolable salt.

Keywords: cycloaddition; cheletropic reaction; quinodimethane; silylene; corannulene; dearomatization; silepin; diradical; radical anion

check for updates

Academic Editor: Igor Alabugin

Received: 12 February 2025
Revised: 5 March 2025
Accepted: 6 March 2025
Published: 11 March 2025

Citation: Ishida, S.; Mori, M.; Honda, S.; Iwamoto, T. A Stable π-Expanded *o*-Quinodimethane via the Photochemical Dearomative Cycloaddition of Corannulene with an Isolable Dialkylsilylene. *Chemistry* **2025**, *7*, 37. https://doi.org/10.3390/chemistry7020037

Copyright: © 2025 by the authors. Licensee MDPI, Basel, Switzerland. This article is an open access article distributed under the terms and conditions of the Creative Commons Attribution (CC BY) license (https://creativecommons.org/licenses/by/4.0/).

1. Introduction

o-Quinodimethanes (*o*QDMs) are important reactive dienes to construct benzo-fused cyclic skeletons by cycloaddition, and their properties have received wide attention [1–5]. Recent sophisticated synthetic methods and molecular design provide stable *o*QDM derivatives, and their electronic structure, involving diradical character due to the narrow HOMO-LUMO gap, has been revealed. oQDMs **A** reported by Suzuki exhibit redox systems associating large structural change from nonaromatic oQDM to dications (Figure 1a) [6,7]. Escudié has demonstrated that the cycloaddition of a reactive Ge=C doubly bonded compound [$Mes_2Ge{=}CR_2$ (CR_2 = fluorenylidene)] with 1,4-naphthoquinone yields stable oQDM **B** [8,9]. Tobe and Shimizu have developed the chemistry of indeno [2,1-*a*]fluorene derivatives **C** and **D** as stable oQDMs and their characteristic electronic character [10–12]. These pioneering works contribute deeper understanding of polycyclic aromatic hydrocarbons (PAHs) and the relationship between structures and their diradical character [13]. Nevertheless, the number of stable oQDMs is still limited and new synthetic methods are highly desired [14–17].

Silylenes (divalent silicon species) undergo dearomative cycloaddition with aromatic compounds, producing silicon-containing seven-membered rings [18–30]. This type of reaction, a silicon version of Büchner ring expansion, becomes a powerful tool for constructing nonaromatic π-electron conjugated systems from readily available aromatic compounds in short steps. We have studied the dearomative cycloadditions of benzenes, azulenes, diaryl ketones, and related compounds using an isolable silylene (**1**) [31] and properties of the products, non-benzenoid π-electron conjugated systems [32–36]. For instance, **1** reacts with benzenes under visible light irradiation ($\lambda > 420$ nm) to afford silepins (silacycloheptatrienes) **E**–**H** (Figure 1b) [32]. The formation mechanism of **E** via the singlet excited state of **1** was theoretically investigated [37]. Based on these previous reports, we envisaged the dearomative cycloaddition of corannulene, a bowl-shaped nonplanar hydrocarbon with

C_{5v} symmetry [38,39], with **1** to afford benzo[6,7]fluoranthen[1,10-*cde*]silepin derivative **2** that has a π-expanded oQDM structure. We report herein the detailed synthesis of **2** and its structure, properties, reaction with O_2, and one-electron reduction (Figure 1c).

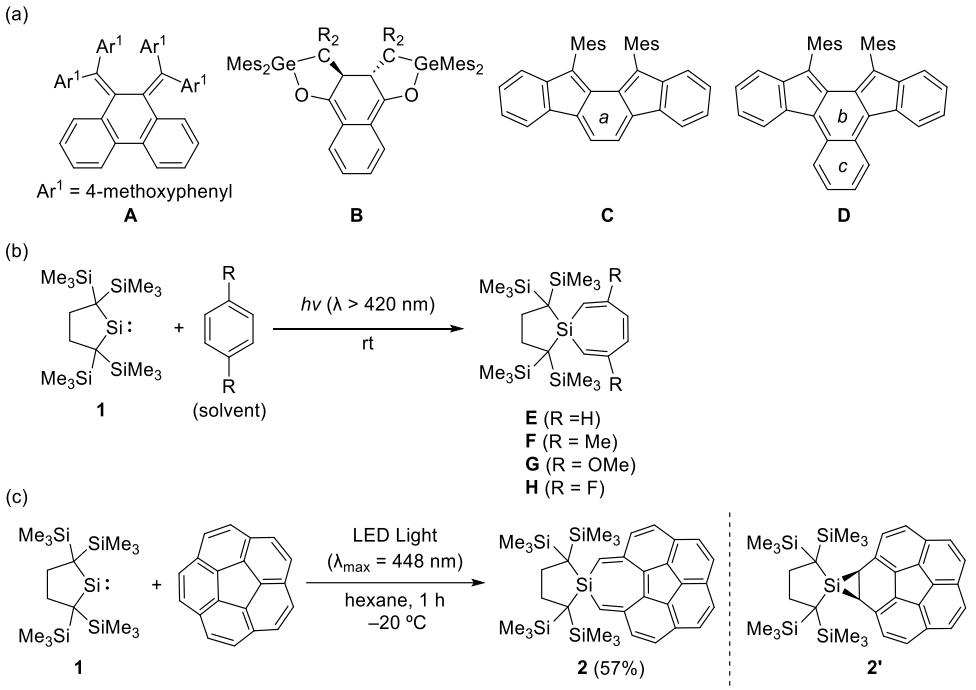


Figure 1. (**a**) Stable oQDMs. (**b**) Photochemical reactions of **1** with benzenes to afford silepins **E**–**H**. (**c**) Synthesis of **2** (this work).

2. Results and Discussion

2.1. Synthesis and Structure

When a hexane solution of corannulene and 1.1 equiv of **1** (λ_{max} = 440 nm) was irradiated by LED light (λ_{max} = 448 nm) at −20 °C, the color of the solution turned from yellow to intense blue within a minute. Further irradiation for 1 h at −20 °C was conducted to complete the reaction. After the recrystallization of the crude product from a saturated hexane solution, cycloadduct **2** was obtained in 57% yield as an air-sensitive dark-blue powder (Figure 1c). The structure of **2** was confirmed by a combination of NMR spectroscopy, MS spectrometry, single crystal X-ray diffraction (sc-XRD) study, and elemental analysis. According to the previous reports on the related reactions of silylenes [18–36], the formation of **2** would proceed via (1 + 2) cycloaddition (cheletropic reaction) to afford silanorcaradiene **2′** and the subsequent electrocyclic ring-opening reaction.

The molecular structure of **2** obtained by sc-XRD is displayed in Figure 2a. The π-electron system of **2** is almost planar. The bowl depth (d_{bowl}), defined as the distance from the center of the hub carbon atoms (C16−C20) to the mean planes of the carbon atoms at the rim positions (C3, C4, C6, C7, C9, C10, C12, C13), is only 0.099 Å for **2**. The d_{bowl} of **2** is much smaller than that of corannulene (d_{bowl} = 0.87 Å). Introducing a seven-membered ring reduces the strain of the corannulene core. Generally, silepins adopt a boat conformation characterized by fold angles θ and φ (Figure 2b). The fold angles of **2** (θ = 17.0° and φ = 4.9°) are smaller than those of silepin **E** (33.0° and 24.5°) [32], which would result from the fused polycyclic aromatic ring system. Intermolecular π-stacking was found to form a dimeric structure (Figure 2c); the shortest distance between the mean planes of C(sp^2) atoms is 3.45 Å. As shown in Figure 2d, the C(sp^2)–C(sp^2) bond lengths of **2** support the silepin structure, but small bond alternation is found around aromatic rings; the C1–C2/C14–C15 and C16–C20 bond lengths [1.373(3)/1.381(3) and 1.419(3) Å] of **2** are

longer than those of the corresponding parts of silepin **E** [1.335(3)/1.346(4) and 1.332(3) Å], while C2–C16/C14–C20 bonds [1.428(3)/1.431(3) Å] are shortened compared to those of **E** [1.453(4)/1.445(5) Å]. The harmonic oscillator model of aromaticity (HOMA) indices [40,41] for rings A and D (0.77 and 0.80) exhibit their aromatic character, but their degrees are smaller than those for rings B and C (0.95 and 0.95). The HOMA indices of *o*QDM units of **2** are larger than those of ring *a* in **C** (0.65) and rings *b* and *c* in **D** (0.71 and 0.81) [10,11]. These structural characteristics indicate that **2** represents a resonance hybrid of a silepin as π-expanded *o*QDM **2a** and open-shell diradical **2b** due to the recovery of two Clar's sextet (Figure 2e) [42–44]. ^{1}H NMR spectrum of **2** exhibits a diamagnetic character of **2**. ^{1}H NMR spectrum of **2** in C_6D_6 shows sharp two singlet peaks (0.20 and 1.98 ppm) with a ratio of 36:4 in the aliphatic region due to four trimethylsilyl groups and the methylene protons on the silacyclopentane, which indicates a facile boat-to-boat inversion in NMR time scale. In the aromatic region of the ^{1}H NMR spectrum of **2**, four doublet signals and a sharp singlet signal appeared with a ratio of 2:2:2:2:2. The singlet signal due to protons on C1/C15 atoms was located at 6.56 ppm, but in ^{13}C NMR, the tertiary C1/C15 signals at 132.6 ppm is considerably broadened compared to the other signals (Figure S2). The observed signal broadening may be due to the contribution of the open-shell character of **2b**.

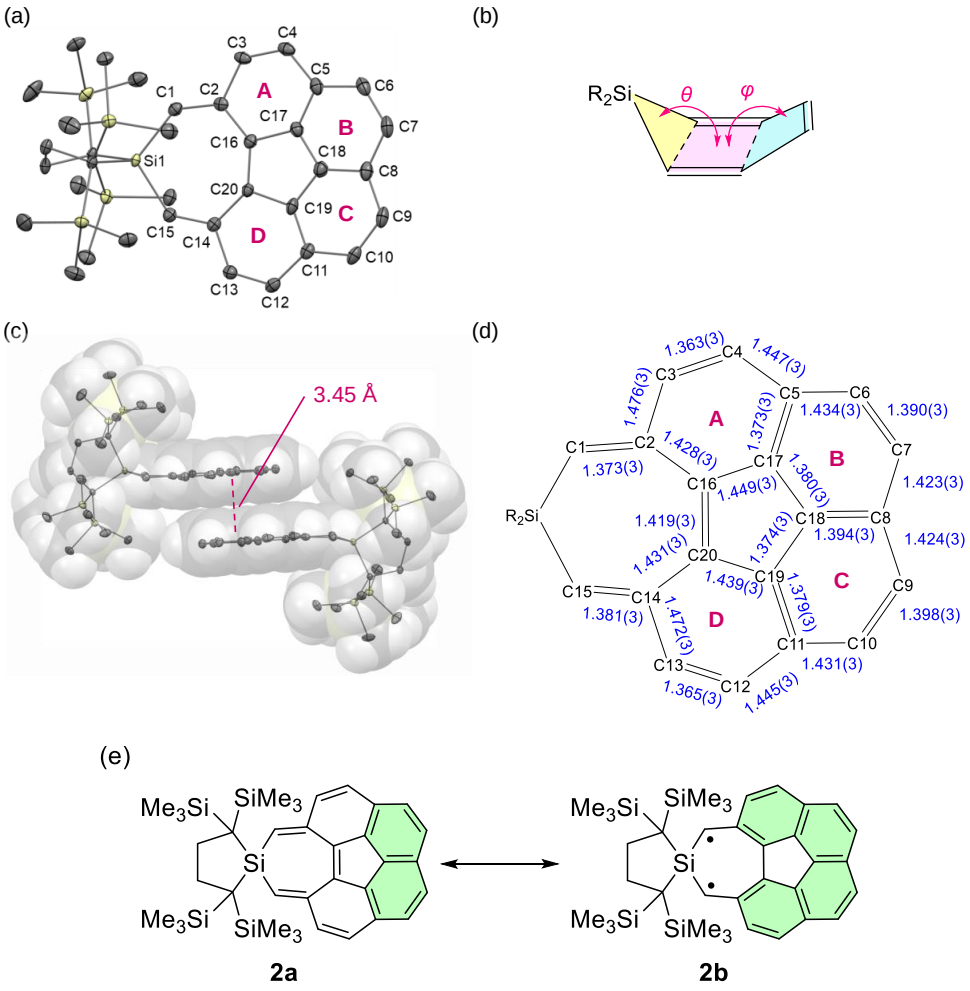


Figure 2. (**a**) ORTEP of **2**. Atomic displacement parameters are set at 50% probability. Hydrogen atoms are omitted for clarity. (**b**) Schematic representation of fold angles θ and φ. (**c**) Dimeric structure of **2** in the solid state with π-contact and the shortest distances between two mean planes of C(sp^2) atoms. (**d**) Selected bond lengths (Å) of **2**. (**e**) Resonance structures of **2**. Green aromatic rings indicate Clar's sextet.

2.2. UV-vis Absorption Spectrum and Electronic Structure

The Uv-vis spectrum of **2** in hexane exhibits four absorption bands associated with vibronic structures (Figure 3a). Characteristic absorption bands in the visible region (band-I: 673 nm and band-II: 502 nm) are not found in silepins **E**–**H** or corannulene. To obtain insight into the electronic structure of **2**, we carried out TD-DFT calculations for the optimized structure of **2** ($\mathbf{2_{opt}}$) at the B3PW91/6-31+G(d,p)//B3LYP-D3/6-31G(d) level of theory, and the frontier orbitals of the optimized structure of $\mathbf{2_{opt}}$ are shown in Figure 3b. Based on the band positions, band-I is assignable to the HOMO–LUMO transition and band-II is attributed to overlapped HOMO-1–LUMO and HOMO-2–LUMO transitions. The HOMO and LUMO are π- and π^*-orbitals delocalized on the π-system and are mainly located on the silepin moiety (Figure 3b). The estimated HOMO-LUMO gap of 2.18 eV is relatively small due to the π-expanded *o*-QDM structure of **2**. HOMO-1 and HOMO-2 are also delocalized over the rings A–D. As the structural characteristics and narrow HOMO–LUMO gap suggest a contribution of diradical character, we conducted further calculations to estimate the diradical index (y_0) using Yamaguchi's method at the LC-(U)BLYP/6-311G(d) level of theory [45–47]. Based on the natural orbital occupation number (NOON) of HONO (1.608) and LUNO (0.392) of the broken symmetry state of **2** ($\mathbf{2_{BS}}$), the approximately spin projected diradical index y_0 is 0.11. Thus, the obtained y_0 value of **2** is much smaller than those of indeno[2,1-*a*]fluorene derivatives **C** (0.33) and **D** (0.63) [10,11]. The small but significant singlet diradical character contributed to the electronic structure of **2**. The triplet state of **2** is 40.7 kJ mol^{-1} above the broken-symmetry singlet state. The contribution of the triplet state to the UV-vis spectrum would be negligible.

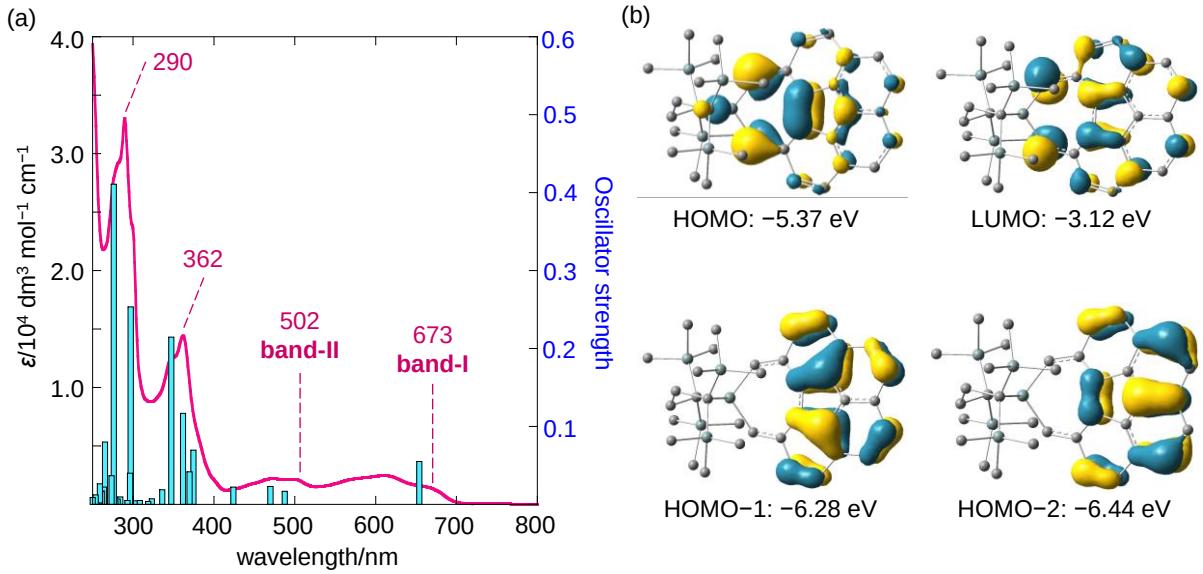
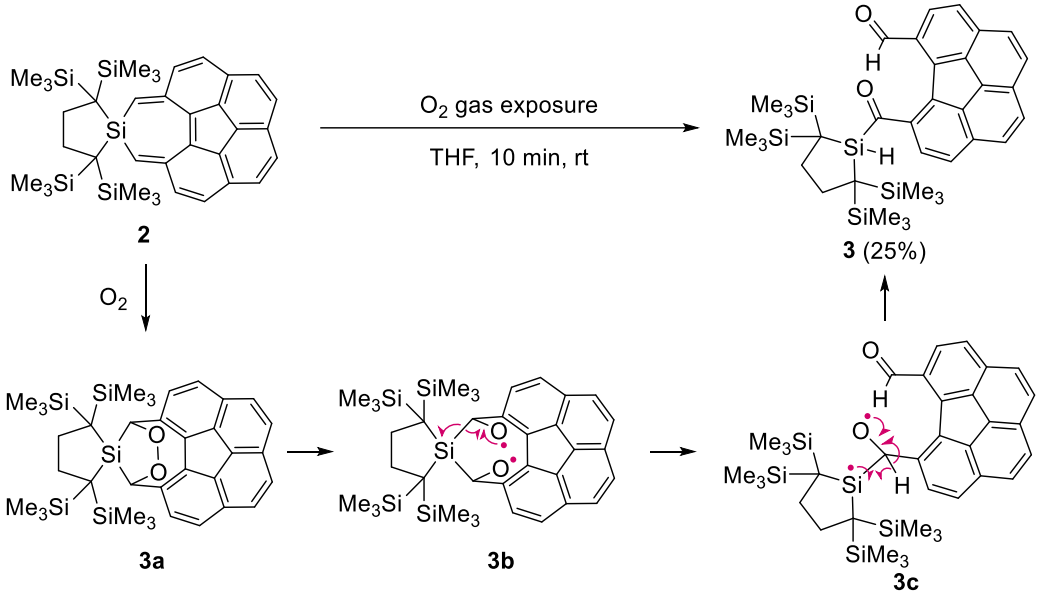


Figure 3. (**a**) UV-vis spectrum of **2** in hexane at room temperature. Superimposed vertical bars indicate band position and oscillator strength of $\mathbf{2_{opt}}$ calculated at the TD-B3PW91/6-31+G(d,p)//B3PW91-D3/6-31G(d) level of theory. The calculated transitions and oscillator strength values are summarized in Table S2 in the supporting information. (**b**) Frontier orbitals of $\mathbf{2_{opt}}$.

2.3. Decomposition of 2 in Air

Corannulene and silepins **E**-**H** are storable in the air, while **2** was readily decomposed to a mixture containing dicarbonyl compound **3**. Even though bulky four trimethylsilyl groups protect the silepin moiety of **2**, facile Si–C bond cleavage occurred via oxidation. Compound **3** was isolated in 25% yield as a yellow solid by the brief exposure of O_2 gas in THF at room temperature for 10 min (Scheme 1). Although the yield should be improved, the selective C=C bond cleavage at the rim position of corannulene to convert benzo[*ghi*]fluoranthene

derivative is achieved in two steps without harsh conditions [48,49]. A proposed formation mechanism is drawn at the bottom of Scheme 1. As several endoperoxides are reported as the product of the reactions of oQDM with oxygen [9,10,12,50], endoperoxide **3a** forms as an initial intermediate in this case. Then, a homolytic O–O bond cleavage of **3a** furnishes diradical **3b**, and the subsequent Si–C bond cleavage to form a formyl group affords **3c**. Finally, forming the strong C=O bond drives a facile 1,2-hydrogen shift of **3c** to give **3**. The molecular structure of **3** was unequivocally determined by sc-XRD (Figure 4).



Scheme 1. Reaction of **2** with O_2 to afford **3** and a proposed formation mechanism.

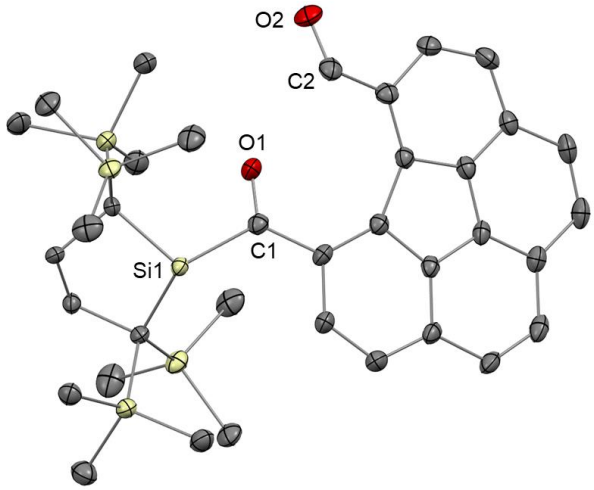


Figure 4. ORTEP of **3**. Hydrogen atoms are omitted for clarity. Thermal ellipsoids are shown at 50% probability level. Crystallographically, two independent molecules exist in the asymmetric unit. As the molecules have almost the same structure, one of them is shown.

2.4. Cyclic Voltammetry and Chemical One-Electron Reduction

Cyclic voltammetry (CV) and differential pulse voltammetry (DPV) of compound **2** at room temperature in THF exhibit three reduction quasi-reversible waves at −1.47, −2.13, and −2.39 V (vs. Fc/Fc^+), respectively (Figure 5). The three-step reduction wave indicates a redox system among neutral, radical anion, dianion, and radical trianion states. The first reduction wave became reversible when the sweep direction was reversed at ca. −1.9 V

(Figure S10a) and is positively shifted by 1.01 V compared to that of corannulene (−2.48 V, see Figure S10b).

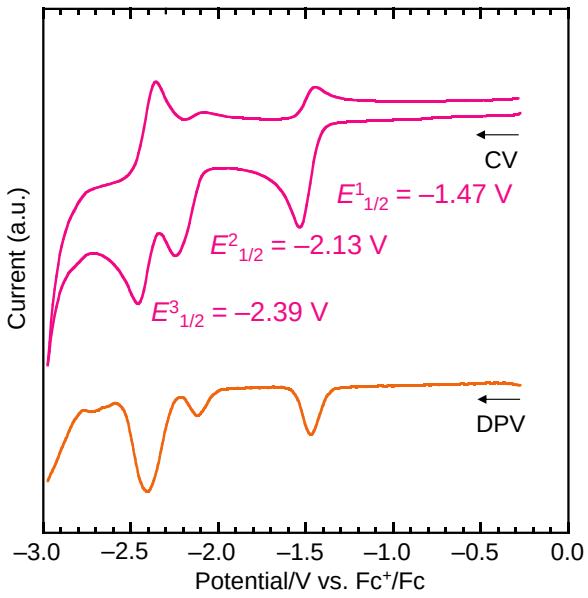


Figure 5. Cyclic voltammogram (CV) and differential pulse voltammogram (DPV) of **2** in THF at room temperature using *n*-$Bu_4N^+[B(C_6F_5)_4]^-$ as an electrolyte (0.1 M), glassy carbon working electrode, and Pt wire counter electrode. For CV: rate = 100 mV s^{-1}. For DPV: pulse width = 50 ms; pulse amplitude = 50 mV; pulse period = 200 ms.

The electrochemical behavior prompted us to conduct the chemical one-electron reduction of **2**; 1.3 equiv of KC_8 was subjected to **2** in the presence of 1 equiv [2.2.2]cryptand in THF for 3 h. The residue did not show significant ^{1}H NMR signals in THF-d_8, suggesting the formation of radical anion $\mathbf{2}^{\bullet-}$. Recrystallization of the residue with a 1:3 mixed solvent of hexane and THF gave radical anion salt [K(222-crypt)]$^+\mathbf{2}^{\bullet-}$ in 58% isolated yield (Figure 6a). The structure was unequivocally determined by sc-XRD and EPR spectroscopy. In the solid state, [K(222-crypt)]$^+\mathbf{2}^{\bullet-}$ exists as a solvent-separated ion pair (Figure 6b), and $\mathbf{2}^{\bullet-}$ has a planar benzo[*ghi*]fluoranthene skeleton. Although the poor quality of the data hampers a detailed discussion on the bond length change upon one-electron reduction of **2**, no intermolecular π-stacking in contrast to the neutral state was found in the solid state.

The ESR spectrum of [K(222-crypt)]$^+\mathbf{2}^{\bullet-}$ in THF at room temperature showed a multiline signal (g = 2.0028, Figure 7a), which was reproduced by computer simulation using three hyperfine coupling constants (hfccs) due to three types of each two hydrogen atoms [$a(^1H^{1/15})$ = 0.655 mT, $a(H^{3/13})$ = $a(^1H^{7/9})$ = 0.202 mT]. (Figure 7b). The isotropic Fermi contact terms obtained by DFT calculation at the UB3PW91/6-31G(d) level of theory of $\mathbf{2}^{\bullet-}$ were 0.87 mT for $H^{1/15}$, 0.27 mT for $H^{3/13}$, 0.25 mT for $H^{7/9}$, respectively, which support the above assignment of hfccs and the structure of $\mathbf{2}^{\bullet-}$ in solution. The SOMO of $\mathbf{2}^{\bullet-}$ that corresponds to the LUMO of **2** is delocalized over the carbon π-system, and the spin density plot of $\mathbf{2}^{\bullet-}$ (Figure 7c) displays that the largest orbital coefficient is on the two carbon atoms adjacent to the silicon atom.

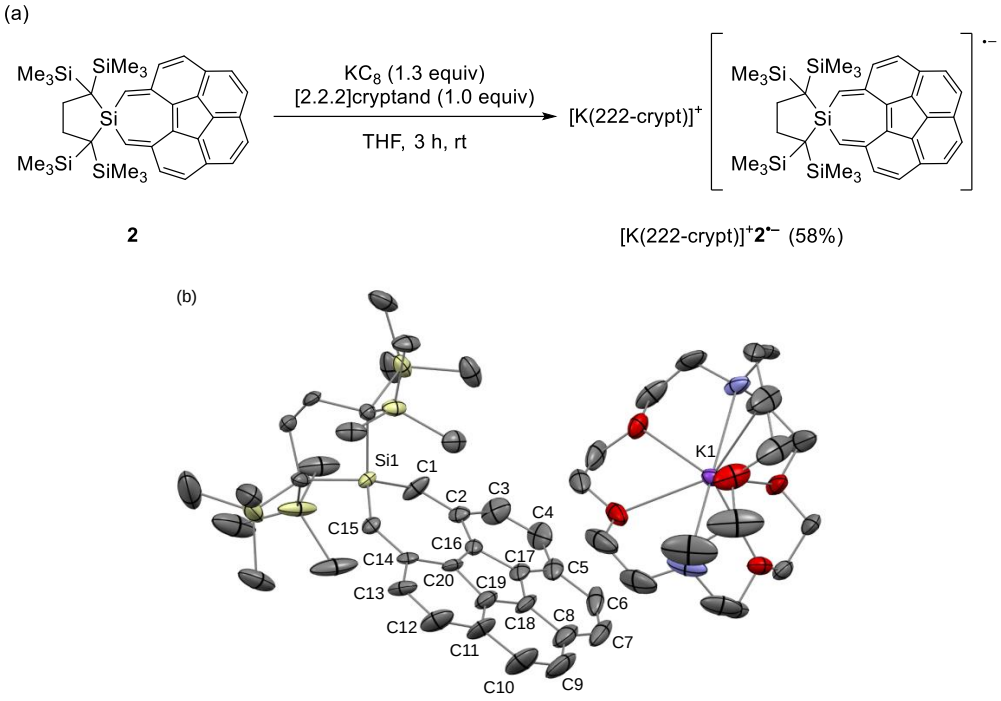


Figure 6. (**a**) One-electron reduction of **2** to afford the corresponding radical anion **2**$^{\bullet-}$. (**b**) Molecular structure of [K(222-crypt)]$^{+}$**2**$^{\bullet-}$. Hydrogen atoms are omitted for clarity. Thermal ellipsoids are shown at 50% probability level.

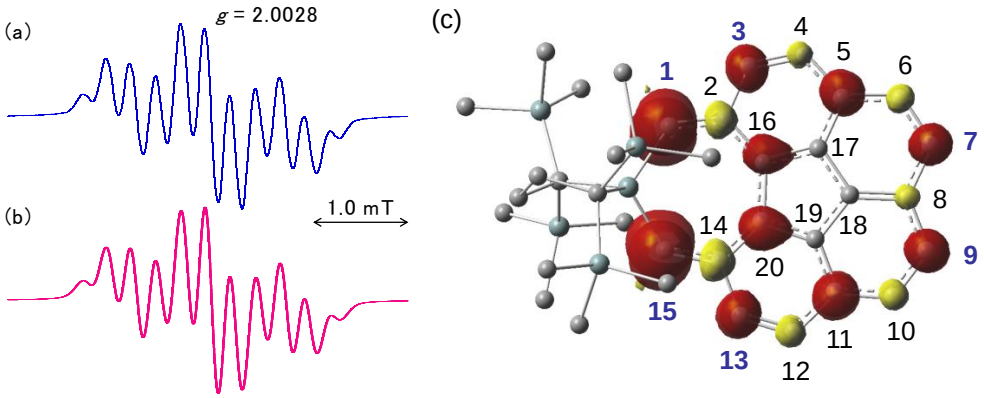


Figure 7. (**a**) EPR spectrum of [K(222-crypt)]$^{+}$**2**$^{\bullet-}$ in THF at room temperature (blue). (**b**) A simulated EPR spectrum of **2**$^{\bullet-}$ using the following parameters (magenta): *g*-value = 2.0028, $a(H^{1/15})$ = 0.202, $a(H^{3/13})$ = 0.202, $a(H^{7/9})$ = 0.655 mT, line width = 0.157 mT, Gaussian-Lorentzian radio = 50:50. (**c**) Computed spin density plot of **2**$^{\bullet-}$ (isosurface value = 0.0024); red and yellow colors represent positive and negative spin density, respectively.

3. Materials and Methods

3.1. General

All reactions treating air- and moisture-sensitive compounds were carried out under argon and nitrogen atmosphere using a high-vacuum line, standard Schlenk techniques, or a glove box, as well as dry and oxygen-free solvents. ^{1}H (500 MHz), ^{13}C (126 MHz), and ^{29}Si (99 MHz) NMR spectra were recorded on a Bruker Avance III 500 FT NMR spectrometer (Bruker Japan, Yokohama, Japan). The ^{1}H NMR chemical shifts were referenced to residual ^{1}H of the solvent: C_6D_6 (^{1}H δ 7.16), $CDCl_3$ (^{1}H δ 7.26). The ^{13}C and ^{29}Si NMR chemical shifts were relative to $SiMe_4$ (δ 0.0) in ppm. Sampling of air-sensitive compounds was carried out using a VAC NEXUS 100027-type glove box (Vacuum Atmospheres Co., Hawthorne, CA, USA). UV-vis spectra were recorded on a JASCO V-660 spectrometer

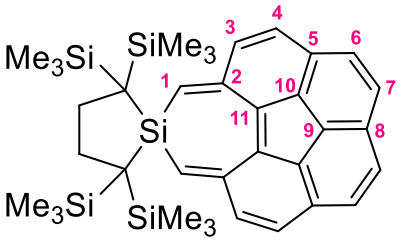
(JASCO, Tokyo, Japan). ESR spectra were recorded on a JEOL X330 ESR spectrometer (JEOL, Tokyo Japan). Photochemical reaction was carried out using a LED light source device (Techno Sigma PER-448 AMP-N1, Okayama, Japan). Cyclic voltammograms (CV) and differential pulse voltammograms (DPV) were recorded on an ECstat-301WL electrochemical analyzer (EC Frontier, Kyoto, Japan). Mass spectra were recorded on a Bruker Daltonics SolariX 9.4T (Bruker Japan, Yokohama, Japan). Melting point was measured using an SRS OptiMelt MPA100 (Stanford Research Systems, Sunnyvale, CA, USA). Elemental analysis was performed with a J-SCIENCE LAB JM-11 (J-SCIENCE, Kyoto, Japan).

3.2. Materials

Dry and degassed hexane and THF were prepared using a VAC 103991 solvent purifier (Vacuum Atmospheres Co., Hawthorne, CA, USA). C_6D_6 and CH_2Cl_2 were degassed by freeze–pump–thaw cycles (three times) and dried over molecular sieves 4 Å. Corannulene and [2.2.2]cryptand were commercially available and used without further purification. 2,2,5,5-Tetrakis(trimethylsilyl)-1-silacyclopentane-1,1-diyl (**1**) was prepared according to procedure described in the literature [31].

3.3. Synthesis of 2′,2′,5′,5′-Tetrakis(trimethylsilyl)spiro[benzo[6,7]fluoranthen[1,10-cde]silepine -2,1′-silolane] (**2**)

In a Schlenk tube (50 mL) equipped with a magnetic stir bar and a glass tube insert having a glass joint and an LED for internal irradiation, corannulene (16 mg, 62 μmol) and 1.1 equiv of silylene **1** (25 mg, 68 μmol) were dissolved in hexane (ca. 5 mL). When the reaction mixture was stirred with irradiation of an LED light source (λ_{max} = 448 nm) at −20 °C, the color of the solution turned yellow of **1** to dark blue of **2** within 1 min. The irradiation was continued for 1 h at −20 °C to complete the reaction. This reaction was performed three times in the same condition. Total amounts of corannulene and **1** are 46 mg (168 μmol) and 75 mg (204 μmol), respectively. After the resulting mixtures were combined and then concentrated in vacuo, the crude product was washed with acetonitrile. Recrystallization of the obtained crude product from hexane at −35 °C produced **2** as dark blue crystals in 57% yield (60 mg, 97 μmol). The color change during the photoirradiation was recorded in Video S1 in the Supplementary Materials. In this video, photoirradiation was conducted at room temperature to clarify the color change.



2

2—dark blue crystal; mp 218–220 °C; ^{1}H NMR (500 MHz, C_6D_6, 298 K, δ) 0.29 (s, 36H, $SiMe_3$), 2.14 (s, 4H, CH_2), 6.56 (s, 2H, H^1), 6.89 (d, J = 18.8 Hz, 2H, $H^{3/4}$), 6.91 (d, J = 18.8 Hz, 2H, $H^{3/4}$), 7.29 (d, J = 8.4 Hz, 2H, $H^{6/7}$), 7.55 (d, J = 8.4 Hz, 2H, $H^{6/7}$); ^{13}C{^{1}H} NMR (126 MHz, C_6D_6, 298 K, δ) 5.3 ($SiMe_3$), 23.4 (C), 35.2 (CH_2), 126.0 ($C^{3/4}H$), 126.1 ($C^{6/7}H$), 126.4 (C), 128.1 (C), 128.2 ($C^{6/7}H$), 130.7 (C), 132.4 (C), 132.6 (broad singlet, C^1H), 136.7 (C), 136.9 ($C^{3/4}H$), 143.3 (C); ^{29}Si{^{1}H} NMR (99 MHz, C_6D_6, 298 K, δ) 2.3 ($SiMe_3$), 9.6 (Si); UV-vis (hexane, rt) λ_{max}, nm (ε): 673 (1.33×10^3), 502 (2.17×10^3), 362 (1.45×10^4), 290 (3.32×10^4); HRMS-APCI (m/z): $[M + H]^+$ calcd for $C_{36}H_{51}Si_5$, 623.2837; found 623.2832; Anal. Calcd for $C_{36}H_{50}Si_5$: C, 68.38; H, 8.09%. Found: C, 68.76; H, 8.22%.

3.4. Synthesis of (2,2,5,5-Tetrakis(trimethylsilyl)silolane-1-carbonyl)benzo[ghi]fluoranthene-5-carbaldehyde (**3**)

In a recovery flask (50 mL), compound **2** (19 mg, 30 μmol) in THF (ca. 5 mL) was placed under O_2 atmosphere for 10 min with stirring. The color of the solution turned from dark blue to yellow. The volatiles were removed in vacuo and the residue was washed with hexane to produce compound **3** as a yellow powder in 25% yield (5 mg, 7.6 μmol).

3—a yellow powder; mp 167–169 °C; ^{1}H NMR (500 MHz, $CDCl_3$, 297 K, δ) 0.20 (s, 18H, $SiMe_3$), 0.26 (s, 18H, $SiMe_3$), 1.97–2.23 (m, 4H, CH_2), 5.30 (s, 1H, SiH), 7.88–7.95 (m, 4H, overlapped signals), 7.97 (d, J = 8.2 Hz, 1H), 8.10 (d, J = 8.2 Hz, 1H), 8.11 (d, J = 8.2 Hz, 1H), 8.48 (d, J = 8.2 Hz, 1H), 10.72 (s, 1H); ^{13}C{^{1}H} NMR (126 MHz, $CDCl_3$, 298 K, δ) 2.1 ($SiMe_3$), 3.8 ($SiMe_3$), 7.0 (C), 33.7 (CH_2), 126.7 (CH), 126.8 (CH), 127.3 (CH), 127.4 (CH) 127.5 (CH), 127.9 (C), 128.0 (CH), 128.5 (CH), 130.2 (C), 130.5 (C), 132.5 (C), 132.8 (CH), 134.0 (C), 134.4 (C), 134.9 (C), 135.1 (C), 138.0 (C), 140.0 (C), 192.8 (CHO), 234.4 (SiC=O); ^{29}Si{^{1}H} NMR (99 MHz, $CDCl_3$, 297 K, δ) –3.7 (Si), 3.8 ($SiMe_3$), 5.0 ($SiMe_3$); MS (EI, 70 eV) m/z (%): 654 (25, M^+), 639 (4, $[M–Me]^+$), 373 (2), 299 (1), 73 (100); Anal. Calcd for $C_{36}H_{50}Si_5O_2$: C, 65.99; H, 7.69%. Found: C, 65.74; H, 7.77%.

3.5. One-Electron Reduction of **2**

In a Schlenk tube (50 mL) equipped with a magnetic stir bar, **2** (15 mg, 24 μmol), [2.2.2]cryptand (9 mg, 24 μmol), and KC_8 (4 mg, 30 μmol) were dissolved in THF (ca. 2 mL). The color of solution turned to reddish brown during stirring at room temperature for 3 h. After the filtration of insoluble materials, volatiles were removed in vacuo. Recrystallization of thus obtained crude from a mixed solution of THF and hexane with a 1:1 ratio afforded $[K(222\text{-crypt})]^+\mathbf{2}^{\bullet-}$ as a brown solid in 58% yield (15 mg, 14 μmol).

$[K(222\text{-crypt})]^+\mathbf{2}^{\bullet-}$: a brown solid; mp 149–153 °C; Anal. Calcd for $C_{54}H_{86}KN_2O_6Si_5$ C, 62.44; H, 8.34%. N, 2.70%. Found: C, 59.39; H, 8.04; N, 2.41%. Elemental analysis of $[K(222\text{-crypt})]^+\mathbf{2}^{\bullet-}$ did not provide satisfactory results due to the extremely air-sensitive nature of $[K(222\text{-crypt})]^+\mathbf{2}^{\bullet-}$, even in the solid state. The pyrophoric nature of solution of $[K(222\text{-crypt})]^+\mathbf{2}^{\bullet-}$ prevented further analysis such as MS spectrometry.

3.6. X-Ray Crystallographic Analysis

Single crystal-X-ray diffraction analysis (sc-XRD) was conducted using a Bruker AXS APEX II CCD diffractometer (Bruker Japan, Yokohama, Japan) with graphite monochromated Mo-Kα radiation. Single crystals, suitable for X-ray diffraction study, were obtained by recrystallization under the following conditions: from hexane at −35 °C for **2**, THF at room temperature **3,** and hexane and THF (3:1) at −35 °C for $[K(222\text{-crypt})]^+\mathbf{2}^{\bullet-}$. The single crystals for data collection coated by Apiezon® grease were mounted on a glass fiber and transferred to the cold nitrogen gas stream of the diffractometer. An empirical absorption correction based on the multiple measurements of equivalent reflections was applied using a program (SADABS, version 2.03) and the structures were solved by direct methods and refined by full-matrix least squares against F^2 using all data (SHELXL-2019) [51,52]. Molecular structure was analyzed by Yadokari-XG software (version 2007.5.12) [53].

Crystal Data of **2** (CCDC 2419073): $C_{36}H_{50}Si_5$; FW 623.21; 100 K; monoclinic; space group $P2_1/n$, a = 9.8555(6) Å, b = 22.0832(13) Å, c = 15.9673(10) Å, β = 93.013(2)°, V = 3470.3(4) Å^3, Z = 4, D_{calc} = 1.193 Mg/m^3, $R1$ = 0.0530 ($I > 2\sigma(I)$), $wR2$ = 0.1253 (all data), GOF = 1.026.

Crystal Data of **3** (CCDC 2419074): $C_{36}H_{50}O_2Si_5$; FW 655.21; 100 K; Triclinic; space group P-1, a = 9.2036(8) Å, b = 11.5218(10) Å, c = 36.978(3) Å, α = 95.551(2)°, β = 90.183(2)°, γ = 113.327(2)°, V = 3580.1(5) Å^3, Z = 4, D_{calc} = 1.216 Mg/m^3, $R1$ = 0.0591 ($I > 2\sigma(I)$), $wR2$ = 0.1333 (all data), GOF = 1.008.

Crystal Data of [K(222-crypt)]$^{+}$**2**$^{\bullet-}$ (CCDC 2419075): $C_{54}H_{85}KN_2O_6Si_5$; FW 1037.78; 100 K; Monoclinic; space group $P2_1/n$, a = 10.4531(17) Å, b = 33.929(5) Å, c = 16.349(3) Å, β = 92.229(5)°, V = 5794.1(16) Å^3, Z = 4, D_{calc} = 1.190 Mg/m^3, $R1$ = 0.1030 ($I > 2\sigma(I)$), $wR2$ = 0.2304 (all data), GOF = 1.013.

3.7. Theoretical Calculations

All theoretical calculations were performed using Gaussian 09 [54] and GRRM 14 [55–60] programs. Geometry optimization and frequency analysis of **2** and **2**$^{\bullet-}$ were carried out at the (U)B3PW91-D3/6-31G(d) level of theory. No imaginary frequencies were found in the optimized structures. Atomic coordinates of the optimized structures are listed in the Supplemental Materials. Forty excited states of **2** calculated at the B3PW91/PCM(hexane)/6-31+G(d,p) level of theory.

4. Conclusions

π-expanded silepin **2** was synthesized by photochemical reaction of silylene **1** and corannulene. Compound **2** has an *o*QDM structure with a small but significant singlet diradical character (y_0 = 0.11). The UV-visible absorption spectrum of **2** shows broad absorption bands in the 400–700 nm region due to the narrow HOMO-LUMO gap (2.18 eV) estimated by computational studies. Both the HOMO and LUMO of **2** have large orbital coefficients on the two carbon atoms adjacent to the central silicon atom. Compound **2** reacted with O_2, giving acylsilane **3** via facile Si–C bond cleavage. The electrochemical behavior of **2** was revealed by CV and radical anion **2**$^{\bullet-}$ was synthesized by one-electron reduction of **2** with KC_8 and isolated as [K(222-crypt)]$^{+}$**2**$^{\bullet-}$. The presented synthetic method would offer potential access to unprecedented π-expanded quinoids and diradicaloids.

Supplementary Materials: The following supporting information can be downloaded at: https://www.mdpi.com/article/10.3390/chemistry7020037/s1, Figures S1–S10: NMR spectra of **2** and **3**; Figures S11 and S12: CV and DPV of **2** and corannulene; Table S1: cartesian coordinates and free energy values of optimized structures; Table S2: calculated transitions by TD-DFT; Video S1: color change in the solution during the photochemical reaction at room temperature.

Author Contributions: Conceptualization, S.I.; methodology, S.I.; validation, S.I. and M.M.; formal analysis, M.M. and S.H.; investigation, M.M. and S.H.; resources, M.M.; data curation, S.I. and T.I.; writing—original draft preparation, S.I. and M.M.; writing—review and editing, S.I. and T.I.; visualization, S.I.; supervision, S.I. and T.I.; project administration, S.I.; funding acquisition, S.I. All authors have read and agreed to the published version of the manuscript.

Funding: This work was funded by JSPS KAKENHI [No. JP25708004 (S.I.)] and the research grant from the Shorai Foundation for Science and Technology (S.I.).

Data Availability Statement: All data are contained in the Supplementary Materials.

Acknowledgments: The authors thank Shin-ichiro Kato (The University of Shiga Prefecture) for advice of the calculation of the diradical character.

Conflicts of Interest: The authors declare no conflicts of interest.

Abbreviations

The following abbreviations are used in this manuscript:

Mes	Mesityl
HOMO	Highest occupied molecular orbital
LUMO	Lowest unoccupied molecular orbital
HONO	Highest occupied natural orbital
LUNO	Lowest unoccupied natural orbital

References

1. Martin, N.; Seoane, C.; Hanack, M. Recent Advances in o-Quinodimethane Chemistry. *Org. Prep. Proced. Int.* **1991**, *23*, 237–272. [CrossRef]
2. Segura, J.L.; Martin, N. *o*-Quinodimethanes: Efficient Intermediates in Organic Synthesis. *Chem. Rev.* **1999**, *99*, 3199–3246. [CrossRef]
3. Konishi, A.; Kubo, T. Benzenoid Quinodimethanes. *Top. Curr. Chem.* **2017**, *375*, 83. [CrossRef] [PubMed]
4. Yang, B.; Gao, S. Recent advances in the application of Diels–Alder reactions involving *o*-quinodimethanes, aza-*o*-quinone methides and *o*-quinone methides in natural product total synthesis. *Chem. Soc. Rev.* **2018**, *47*, 7926–7953. [CrossRef]
5. Sun, Z.; Ye, Q.; Chi, C.; Wu, J. Low band gap polycyclic hydrocarbons: From closed-shell near infrared dyes and semiconductors to open-shell radicals. *Chem. Soc. Rev.* **2012**, *41*, 7857–7889. [CrossRef]
6. Iwashita, S.; Ohta, E.; Higuchi, H.; Kawai, H.; Fujiwara, K.; Ono, K.; Takenaka, M.; Suzuki, T. First stable 7,7,8,8-tetraaryl-o-quinodimethane: Isolation, X-ray structure, electrochromic response of 9,10-bis(dianisylmethylene)-9,10-dihydrophenanthrene. *Chem. Commun.* **2004**, 2076–2077. [CrossRef]
7. Suzuki, T.; Sakano, Y.; Iwai, T.; Iwashita, S.; Miura, Y.; Katoono, R.; Kawai, H.; Fujiwara, K.; Tsuji, Y.; Fukushima, T. 7,7,8,8-Tetraaryl-*o*-quinodimethane Stabilized by Dibenzo Annulation: A Helical π-Electron System That Exhibits Electrochromic and Unique Chiroptical Properties. *Chem. Eur. J.* **2013**, *19*, 117–123. [CrossRef] [PubMed]
8. Ghereg, D.; Ech-Cherif El Kettani, S.; Lazraq, M.; Ranaivonjatovo, H.; Schoeller, W.W.; Escudié, J.; Gornitzka, H. An isolable o-quinodimethane and its fixation of molecular oxygen to give an endoperoxide. *Chem. Commun.* **2009**, 4821–4823. [CrossRef]
9. Ghereg, D.; Gornitzka, H.; Ranaivonjatovo, H.; Escudié, J. Reactions of germenes with various naphthoquinones controlled by substituent effects. *Dalton Trans.* **2010**, *39*, 2016–2022. [CrossRef]
10. Shimizu, A.; Tobe, Y. Indeno [2,1-*a*]fluorene: An Air-Stable *ortho*-Quinodimethane Derivative. *Angew. Chem. Int. Ed.* **2011**, *50*, 6906–6910. [CrossRef]
11. Miyoshi, H.; Nobusue, S.; Shimizu, A.; Hisaki, I.; Miyata, M.; Tobe, Y. Benz[*c*]indeno [2,1-*a*]fluorene: A 2,3-naphthoquinodimethane incorporated into an indenofluorene frame. *Chem. Sci.* **2014**, *5*, 163–168. [CrossRef]
12. Shimizu, A.; Nobusue, S.; Miyoshi, M.; Tobe, Y. Indenofluorene congeners: Biradicaloids and beyond. *Pure Appl. Chem.* **2014**, *86*, 517–528. [CrossRef]
13. Abe, M. Diradicals. *Chem. Rev.* **2013**, *113*, 7011–7088. [CrossRef] [PubMed]
14. Sato, C.; Suzuki, S.; Kozaki, M.; Okada, K. 2,11-Dibromo-13,14-dimesityl-5,8-dioxapentaphene: A Stable and Twisted Polycyclic System Containing the *o*-Quinodimethane Skeleton. *Org. Lett.* **2016**, *18*, 1052–1055. [CrossRef] [PubMed]
15. Adachi, K.; Hirose, S.; Ueda, Y.; Uekusa, H.; Hamura, T. Thermodynamically Stable *o*-Quinodimethane: Synthesis, Structure, and Reactivity. *Chem. Eur. J.* **2021**, *27*, 3665–3669. [CrossRef]
16. Ariai, J.; Gellrich, U. An Acceptor-Substituted *N*-Heterocyclic *ortho*-Quinodimethane: Pushing the Boundaries of Polarization in Donor−Acceptor Substituted Polyenes. *J. Am. Chem. Soc.* **2024**, *146*, 32859–32869. [CrossRef]
17. Sahara, K.; Abe, M.; Zipse, H.; Kubo, T. Duality of Reactivity of a Biradicaloid Compound with an *o*-Quinodimethane Scaffold. *J. Am. Chem. Soc.* **2020**, *142*, 5408–5418. [CrossRef]
18. Zhu, H.; Fujimori, S.; Kostenko, A.; Inoue, S. Dearomatization of C 6 Aromatic Hydrocarbons by Main Group Complexes. *Chem. Eur. J.* **2023**, *29*, e202301973. [CrossRef]
19. Suzuki, H.; Tokitoh, N.; Okazaki, R. A Novel Reactivity of a Silylene: The First Examples of [1 + 2] Cycloaddition with Aromatic Compounds. *J. Am. Chem. Soc.* **1994**, *116*, 11572–11573. [CrossRef]
20. Lim, Y.M.; Lee, M.E.; Lee, J.; Do, Y. Reactivity of Bromodilithiosilane to Naphthalene and Anthracene. *Organometallics* **2008**, *27*, 6375–6378. [CrossRef]
21. Mizuhata, Y.; Sato, T.; Tokitoh, N. Reactions of an overcrowded silylene with pyridines: Formation of a novel 2H-1,2-azasilepine and its further cycloaddition. *Heterocycles* **2012**, *84*, 413–418. [CrossRef]
22. Kosai, T.; Ishida, S.; Iwamoto, T. A Two-Coordinate Cyclic (Alkyl)(Amino)Silylene: Balancing Thermal Stability and Reactivity. *Angew. Chem. Int. Ed.* **2016**, *55*, 15554–15558. [CrossRef]
23. Wendel, D.; Porzelt, A.; Herz, F.A.D.; Sarkar, D.; Jandl, C.; Inoue, S.; Rieger, B. From Si(II) to Si(IV) and Back: Reversible Intramolecular Carbon–Carbon Bond Activation by an Acyclic Iminosilylene. *J. Am. Chem. Soc.* **2017**, *139*, 8134–8137. [CrossRef] [PubMed]
24. Zhu, L.; Zhang, J.; Yang, H.; Cui, C. Synthesis of Silaketenimine Anion and Its Coupling with Isocyanide. *J. Am. Chem. Soc.* **2019**, *141*, 19600–19604. [CrossRef] [PubMed]
25. Zhu, L.; Zhang, J.; Cui, C. Intramolecular Cyclopropanation of Alkali-Metal-Substituted Silylene with the Aryl Substituent of an N-Heterocyclic Framework. *Inorg. Chem.* **2019**, *58*, 12007–12010. [CrossRef]
26. Holzner, R.; Reiter, D.; Frisch, P.; Inoue, S. DMAP-stabilized bis(silyl)silylenes as versatile synthons for organosilicon compounds. *RSC Adv.* **2020**, *10*, 3402–3406. [CrossRef]

27. Reiter, D.; Frisch, P.; Wendel, D.; Hörmann, F.M.; Inoue, S. Oxidation reactions of a versatile, two-coordinate, acyclic iminosiloxysilylene. *Dalton Trans.* **2020**, *49*, 7060–7068. [CrossRef]
28. Xu, C.; Ye, Z.; Xiang, L.; Yang, S.; Peng, Q.; Leng, X.; Chen, Y. Insertion of Metal-Substituted Silylene into Naphthalene's Aromatic Ring and Subsequent Rearrangement for Silaspiro-Benzocycloheptenyl and Cyclobutenosilaindan Derivatives. *Angew. Chem. Int. Ed.* **2021**, *60*, 3189–3195. [CrossRef]
29. Zhu, H.; Kostenko, A.; Franz, D.; Hanusch, F.; Inoue, S. Room Temperature Intermolecular Dearomatization of Arenes by an Acyclic Iminosilylene. *J. Am. Chem. Soc.* **2023**, *145*, 1011–1021. [CrossRef]
30. Ding, Y.; Jin, W.; Zhang, J.; Cui, C. A Masked Boryl-Substituted Oxo-Bridged Bis-Silylene: Synthesis and Reductive-Elimination and Synergistic Oxidative-Addition Reactivity. *J. Am. Chem. Soc.* **2024**, *146*, 27925–27934. [CrossRef]
31. Kira, M.; Ishida, S.; Iwamoto, T.; Kabuto, C. The First Isolable Dialkylsilylene. *J. Am. Chem. Soc.* **1999**, *121*, 9722–9723. [CrossRef]
32. Kira, M.; Ishida, S.; Iwamoto, T.; Kabuto, C. Excited-State Reactions of an Isolable Silylene with Aromatic Compounds. *J. Am. Chem. Soc.* **2002**, *124*, 3830–3831. [CrossRef]
33. Kira, M.; Ishida, S.; Iwamoto, T.; de Meijere, A.; Fujitsuka, M.; Ito, O. The Singlet Excited State of a Stable Dialkylsilylene is Responsible for Its Photoreactions. *Angew. Chem. Int. Ed. Engl.* **2004**, *43*, 4510–4512. [CrossRef] [PubMed]
34. Fukuoka, T.; Uchida, K.; Sung, Y.M.; Shin, J.-Y.; Ishida, S.; Lim, J.M.; Hiroto, S.; Furukawa, K.; Kim, D.; Iwamoto, T.; et al. Near-IR Absorbing Nickel(II) Porphyrinoids Prepared by Regioselective Insertion of Silylenes into Antiaromatic Nickel(II) Norcorrole. *Angew. Chem. Int. Ed.* **2014**, *53*, 1506–1509. [CrossRef]
35. Kosai, T.; Ishida, S.; Iwamoto, T. Transformation of azulenes to bicyclic [4]dendralene and heptafulvene derivatives by photochemical cycloaddition of dialkylsilylene. *Chem. Commun.* **2015**, *51*, 10707–10709. [CrossRef] [PubMed]
36. Ishida, S.; Tamura, T.; Iwamoto, T. Dearomative cycloadditions of a silylene with pyrazine and quinoxaline. *Dalton Trans.* **2018**, *47*, 11317–11321. [CrossRef]
37. Su, M.-D. A Theoretical Investigation of Photochemical Reactions of an Isolable Silylene with Benzene. *Chem. Eur. J.* **2014**, *20*, 9419–9423. [CrossRef]
38. Li, X.; Kang, F.; Inagaki, M. Buckybowls: Corannulene and Its Derivatives. *Small* **2016**, *12*, 3206–3223. [CrossRef]
39. Nestoros, E.; Stuparu, M.C. Corannulene: A molecular bowl of carbon with multifaceted properties and diverse applications. *Chem. Commun.* **2018**, *54*, 6503–6519. [CrossRef]
40. Krygowski, T.M.; Cyrański, M.K. Structural aspects of aromaticity. *Chem. Rev.* **2001**, *101*, 1385–1419. [CrossRef]
41. Krygowski, T.M.; Szatylowicz, H.; Stasyuk, O.A.; Dominikowska, J.; Palusiak, M. Aromaticity from the viewpoint of molecular geometry: Application to planar systems. *Chem. Rev.* **2014**, *114*, 6383–6422. [CrossRef]
42. Clar, E. *The Aromatic Sextet*; Wiley: London, UK, 1972.
43. Balaban, A.T.; Klein, D.J. Claromatic Carbon Nanostructures. *J. Phys. Chem. C* **2009**, *113*, 19123–19133. [CrossRef]
44. Wassmann, T.; Seitsonen, A.P.; Saitta, A.M.; Lazzeri, M.; Mauri, F. Clar's Theory, Pi-Electron Distribution, and Geometry of Graphene Nanoribbons. *J. Am. Chem. Soc.* **2010**, *132*, 3440–3451. [CrossRef] [PubMed]
45. Nakano, M.; Kishi, R.; Nitta, T.; Kubo, T.; Nakasuji, K.; Kamada, K.; Ohta, K.; Yamaguchi, K. Second Hyperpolarizability (γ) of Singlet Diradical System: Dependence of γ on the Diradical Character. *J. Phys. Chem. A* **2005**, *109*, 885–891. [CrossRef] [PubMed]
46. Kamada, K.; Ohta, K.; Shimizu, A.; Kubo, T.; Kishi, R.; Takahashi, H.; Botek, E.; Champagne, B.; Nakano, M. Singlet Diradical Character from Experiment. *J. Phys. Chem. Lett.* **2010**, *1*, 937–940. [CrossRef]
47. Nakano, M. Electronic Structure of Open-Shell Singlet Molecules: Diradical Character Viewpoint. *Top. Curr. Chem.* **2017**, *375*, 47. [CrossRef]
48. Tashiro, S.; Yamada, M.; Shionoya, M. Iridium-Catalyzed Reductive Carbon–Carbon Bond Cleavage Reaction on a Curved Pyridylcorannulene Skeleton. *Angew. Chem. Int. Ed.* **2015**, *54*, 5351–5354. [CrossRef]
49. Guo, W.; Ding, W.; Yao, Y.; Rajca, S.; Li, Q.; Jiang, H.; Rajca, A.; Wang, Y. Aromatic C−C Bond Cleavage in a Curved π-System of Aminocorannulene. *Org. Lett.* **2023**, *25*, 3972–3977. [CrossRef]
50. Balci, M. Bicyclic Endoperoxides and Synthetic Applications. *Chem. Rev.* **1981**, *81*, 91–108. [CrossRef]
51. Sheldrick, G.M. *SADABS, Empirical Absorption Correction Program*; University of Göttingen: Göttingen, Germany, 1996.
52. Sheldrick, G.M. *SHELXL-2019, Program for the Refinement of Crystal Structures*; University of Göttingen: Göttingen, Germany, 2019.
53. Kabuto, C.; Akine, S.; Nemoto, T.; Kwon, E. Release of Software (Yadokari-XG 2009) for Crystal Structure Analyses. *J. Cryst. Soc. Jpn.* **2009**, *51*, 218–224. [CrossRef]
54. Frisch, M.J.; Trucks, G.W.; Schlegel, H.B.; Scuseria, G.E.; Robb, M.A.; Cheeseman, J.R.; Scalmani, G.; Barone, V.; Mennucci, B.; Petersson, G.A.; et al. *Gaussian 09, Revision D.01*; Gaussian, Inc.: Wallingford, CT, USA, 2009.
55. Maeda, S.; Ohno, K.; Morokuma, K. Systematic exploration of the mechanism of chemical reactions: The global reaction route mapping (GRRM) strategy using the ADDF and AFIR methods. *Phys. Chem. Chem. Phys.* **2013**, *15*, 3683–3701. [CrossRef] [PubMed]
56. Ohno, K.; Maeda, S. A scaled hypersphere search method for the topography of reaction pathways on the potential energy surface. *Chem. Phys. Lett.* **2004**, *384*, 277–282. [CrossRef]

57. Maeda, S.; Ohno, K. Global Mapping of Equilibrium and Transition Structures on Potential Energy Surfaces bythe Scaled Hypersphere Search Method: Applications to ab Initio Surfaces of Formaldehyde and Propyne Molecules. *J. Phys. Chem. A* **2005**, *109*, 5742–5753. [CrossRef] [PubMed]
58. Ohno, K.; Maeda, S. Global Reaction Route Mapping on Potential Energy Surfaces of Formaldehyde, Formic Acid, and Their Metal-Substituted Analogues. *J. Phys. Chem. A* **2006**, *110*, 8933–8941. [CrossRef]
59. Maeda, S.; Ohno, K. Structures of Water Octamers $(H_2O)_8$: Exploration on Ab Initio Potential Energy Surfaces by the Scaled Hypersphere Search MethodClick to copy article link. *J. Phys. Chem. A* **2007**, *111*, 4527–4534. [CrossRef]
60. Maeda, S.; Harabuchi, Y.; Osada, Y.; Taketsugu, T.; Morokuma, K.; Ohno, K. GRRM14. Available online: https://iqce.jp/GRRM/index_e.shtml (accessed on 24 September 2020).

Disclaimer/Publisher's Note: The statements, opinions and data contained in all publications are solely those of the individual author(s) and contributor(s) and not of MDPI and/or the editor(s). MDPI and/or the editor(s) disclaim responsibility for any injury to people or property resulting from any ideas, methods, instructions or products referred to in the content.